Ligand-Stabilized Ruthenium Nanoparticles: Synthesis, Organization, and Dynamics

Cheng Pan,[†] Katrin Pelzer,[†] Karine Philippot,[†] Bruno Chaudret,*[,†] Fabrice Dassenoy,[‡] Pierre Lecante,[‡] and Marie-José Casanove[‡]

Contribution from the Laboratoire de Chimie de Coordination du CNRS, 205, route de Narbonne, 31077 Toulouse Cédex 04, France, and Centre d'Elaboration des Matériaux et d'Etudes Structurales du CNRS, 29, rue Jeanne Marvig, BP 4347, 31055 Toulouse Cédex 04, France

Received November 15, 2000

Abstract: The decomposition of the ruthenium precursor Ru(COD)(COT) (**1**, COD = 1,5-cyclooctadiene; COT = 1,3,5-cyclooctatriene) in mild conditions (room temperature, 1−3 bar H_2) in THF leads, in the presence of a stabilizer (polymer or ligand), to nanoparticles of various sizes and shapes. In THF and in the presence of a polymer matrix (Ru/polymer = 5%), crystalline hcp particles of uniform mean size (1.1 nm) homogeneously dispersed in the polymer matrix and agglomerated hcp particles (1.7 nm) were respectively obtained in poly(vinylpyrrolidone) and cellulose acetate. The same reaction, carried out using various concentrations relative to ruthenium of alkylamines or alkylthiols as stabilizers (L = $C_8H_{17}NH_2$, $C_{12}H_{25}NH_2$, $C_{16}H_{33}NH_2$, $C_8H_{17}SH$, $C_{12}H_{25}SH$, or $C_{16}H_{33}SH$), leads to agglomerated particles (L = thiol) or particles dispersed in the solution (L = amine), both displaying a mean size near 2−3 nm and an hcp structure. In the case of amine ligands, the particles are generally elongated and display a tendancy to form worm- or rodlike structures at high amine concentration. This phenomenon is attributed to a rapid amine ligand exchange at the surface of the particle as observed by ^{13}C NMR. In contrast, the particles stabilized by $C_8H_{17}SH$ are not fluxional, but a catalytic transformation of thiols into disulfides has been observed which involves oxidative addition of thiols on the ruthenium surface. All colloids were characterized by microanalysis, infrared spectroscopy after CO adsorption, high-resolution electron microscopy, and wide-angle X-ray scattering.

There is presently a very large interest in the use of nanoobjects for various applications involving mainly physical properties.[1] However, the physical and chemical properties of nanoparticles depend on several factors, such as (i) the particle size and the size dispersity; (ii) the structure of the particles; (iii) the surface of the particles; (iv) the shape of the particles; and (v) the organization of the particles into a nanomaterial and their dispensability. In turn, these factors will depend on the successful control, including reproducibility, of the synthetic process and the stability of the particles. The most common tools used for stabilizing nanoparticles have been so far polymers, but they may not be usable in selected chemical or physical applications. For this reason, the use of ligands coordinated at the surface of the particles has been considerably developed in the past few years.[2−9] The presence of ligands prevents the particles from coalescing and allows their self-assembly onto various surfaces. Long-chain thiols[3,4] are the most commonly used ligands, but phosphines,[2,5] pyridine derivatives,[2,6] trioctylphosphine oxide (TOPO),[7] and long-chain amines[3d,8] have also been employed for stabilizing metal nanoparticles, in most cases gold nanoparticles.[2,3,6,8a,b] However, only a few studies have addressed the problem of the coordination mode of the ligand on the particles using molecular chemistry

* To whom correspondence should be addressed. E-mail: chaudret@lcc-toulouse.fr.

† Laboratoire de Chimie de Coordination du CNRS.

‡ Centre d'Elaboration des Matériaux et d'Etudes Structurales du CNRS.

(1) See for example: (a) Alivisatos, A. P. *Science* **1996**, *271*, 933. (b) Schön, G.; Simon, U. *Colloid Polym. Sci.* **1995**, *273*, 101. (c) Fendler, J. H. *Chem. Mater.* **1996**, *8*, 1616 and references therein. (d) Colvin, V. L.; Schlamp, M. P.; Alivisatos, A. P. *Nature* **1994**, *370*, 354. (e) Rao, C. N. R.; Kulkarni, G. U.; Thomas, P. J.; Edwards, P. P. *Chem. Soc. Rev.* **2000**, *29*, 27. (f) Wang, Z. L. *Adv. Mater.* **1998**, *10*, 13.

(2) (a) Schmid, G.; Maihack, V.; Lantermann, F.; Peschel, S. *J. Chem. Soc., Dalton Trans.* **1996**, 589. (b) Schmid, G.; Bäumle, M.; Geerkens, M.; Heim, I.; Osemann, C.; Sawitowski, T. *Chem. Soc. Rev.* **1999**, 179.

(3) (a) Fink, J.; Kiely, C. C. J.; Bethell, D.; Schiffrin, D. J. *Chem. Mater.* **1998**, *10*, 922. (b) Chen, S.; Murray, R. W. *Langmuir* **1999**, *15*, 682. (c) Chechick, V.; Crooks, R. M. *Langmuir* **1999**, *15*, 6364. (d) Lin, X. M.; Wang, G. M.; Sorensen, C. M.; Klabunde, K. J. *J. Phys. Chem. B* **1999**, *103*, 5488.

(4) (a) Ohara, P. C.; Heath, J. R.; Gelbart, W. M. *Angew. Chem., Int. Ed.* **1997**, *36*, 1078. (b) Korgel, B. A.; Fitzmaurice, D. *Adv. Mater.* **1998**, *10*, 661. (c) Taleb, A.; Petit, C.; Pileni, M.-P. *J. Phys. Chem. B* **1998**, *102*, 2215. (d) Petit, C.; Taleb, A.; Pileni, M.-P. *J. Phys. Chem. B* **1999**, *103*, 1805. (e) Yee, C. K.; Jordan, R.; Ulman, A.; White, H.; King, A.; Rafailovitch, M.; Sokolov, J. *Langmuir* **1999**, *15*, 3486. (f) Dassenoy, F.; Philippot, K.; Ould Ely, T.; Amiens, C.; Lecante, P.; Snoeck, E.; Mosset, A.; Casanove, M.-J.; Chaudret B. *New J. Chem.* **1998**, *22*, 703.

(5) Rodriguez, A.; Amiens, C.; Chaudret, B.; Casanove, M.-J.; Lecante, P.; Bradley, J. S. *Chem. Mater.* **1996**, *8*, 1978.

(6) Naka, K.; Yaguchi, M.; Chujo, Y. *Chem. Mater.* **1999**, *11*, 849.

(7) (a) Shenton, W.; Pum, D.; Sleytr, U. B.; Mann, S. *Nature* **1997**, *389*, 585. (b) Cassagneau, T.; Mallouk, T. E.; Fendler, J. H. *J. Am. Chem. Soc.* **1998**, *120*, 7848. (c) Soulantika, K.; Maisonnat, A.; Chaudret, B.; Fromen, M.-C.; Casanove, M.-J.; Lecante, P. *Angew. Chem., Int. Ed.*, in press.

(8) (a) Yonezawa, T.; Tominaga, T.; Richard, D. *J. Chem. Soc., Dalton Trans.* **1996**, 783. (b) Sato, T.; Brown, D.; Johnson, B. F. G. *J. Chem. Soc., Chem. Commun.* **1997**, 1007. (c) Gomez, S.; Philippot, K.; Colliere, V.; Chaudret, B.; Senocq, F.; Lecante, P. *J. Chem. Soc., Chem. Commun.* **2000**, 1945.

(9) (a) Terrill, R. H.; Postlethwaite, T. A.; Chen, C.-H.; Poon, C.-D.; Terzis, A.; Chen, A.; Hutchison, J. E.; Clark, M. R.; Wignall, G.; Londono, J. D.; Superfine, R.; Falvo, M.; Johnson, C. S., Jr.; Samulski, E. T.; Murray, R. W. *J. Am. Chem. Soc.* **1995**, *117*, 12537. (b) Badia, A.; Gao, W.; Singh, S.; Demers, L.; Cuccia, L.; Reven, L. *Langmuir* **1996**, *12*, 1262. (c) Badia, A.; Cuccia, L.; Demers, L.; Morin, F.; Lennox, R. B. *J. Am. Chem. Soc.* **1997**, *119*, 2682. (d) Hostetler, M. J.; Wingate, J. E.; Zhong, C.-J.; Harris, J. E.; Vachet, R. W.; Clark, M. R.; Londono, J. D.; Green, S. J.; Stokes, J. J.; Wignall, G. D.; Glish, G. L.; Porter, M. D.; Evans, N. D.; Murray, R. W. *Langmuir* **1998**, *14*, 17.

10.1021/ja003961m CCC: $20.00
Published on Web 07/14/2001

techniques such as ^{1}H and ^{13}C NMR and FTIR.[9] These techniques are expected to demonstrate the presence of the ligand on the surface of the particles but could also give an idea of the energetics and the dynamics of the ligand's coordination.

We started some years ago a program aiming at synthesizing nanoparticles using the tools of organometallic synthesis.[4f,5,7c,8c,10,11] Organometallic derivatives may provide a general route for the synthesis of monodisperse nanoparticles, as recently illustrated.[12] In our case the decomposition is carried out in mild conditions in the presence of a reactive gas, CO or H_2. We have been interested in ruthenium, which is a metal of catalytic interest and a precursor for semiconducting oxides but for which the literature remains very limited.[13] We have, for example, shown that the decomposition of the ruthenium precursor Ru(COD)(COT)[14] (**1**, COD = 1,5-cyclooctadiene; COT = 1,3,5-cyclooctatriene) could be carried out in mild conditions (room temperature, 1−3 bar H_2) in THF to yield nanoparticles of various sizes and shapes.[10] We have also demonstrated in the case of cobalt that this technique allows the particles to display the same physical surface properties as particles prepared in high vacuum.[11] We describe in this paper the preparation of ligand-protected ruthenium nanoparticles, the study of the influence of the ligands on the size and shape of the nanoparticles, and their characterization both by material characterization techniques (electron microscopy, X-ray scattering) and by solution NMR studies. The synthesis in a polymer matrix of regularly dispersed nanoparticles of uniform size (1.2 nm in PVP) has been reported in a preliminary account.[10b]

Decomposition of Ru(COD)(COT) in a Polymer

Before studying the decomposition of the ruthenium precursor Ru(COD)(COT) in the presence of ligands, we investigated the reaction in the same conditions of solvent, temperature, and dihydrogen pressure but in the presence of a polymer. We have previously reported the decomposition of this precursor in the presence of various polymers,[15] and the decomposition in poly(vinylpyrrolidone) (PVP) has recently been mentioned in a preliminary publication dealing with the synthesis of bimetallic particles.[10b] The reaction of **1** in THF in the presence of PVP or cellulose acetate (CAC; [Ru]/polymer, 5 wt %) with 3 bar dihydrogen at 193 K for 15 h leads to a homogeneous brown solution. Addition of pentane leads to the precipitation of a brown powder which can then be dissolved in methanol and precipitated with pentane.

The colloids were characterized by microanalysis and infrared spectroscopy (IR) after adsorption of CO, high-resolution electron microscopy (HREM), and wide-angle X-ray scattering (WAXS). The ruthenium contents of the colloids were found to be respectively 7.6 (PVP) and 4.3 wt % (CAC). The excess ruthenium found in the PVP colloid is due to the elimination of excess PVP by precipitation and washing. Both colloids display a single CO stretch respectively at 2014 and 2026 cm^{-1}, in agreement with terminal CO groups adsorbed on ruthenium(0).[15] High-resolution electron micrographs show particles homogeneously distributed in the PVP matrix. They display a uniform size centered near 1.1 nm and the hcp structure of bulk ruthenium (see Figures 1 and 2). The radial distribution function (RDF) of the particles (Figure 3) is consistent with the hcp structure and displays a coherence length of ca. 1.1 nm, in agreement with the microscopy results. This result demonstrates the crystallinity of the particles. The metal−metal distance was found to be equal to that in bulk ruthenium (2.670 Å), and the data were simulated using a 100-atom model adopting the hcp structure. This simulation suggests a relaxation of the lattice parameters of the hcp structure: a = 2.66 Å, c = 4.36 Å compared to a = 2.7058 Å and c = 4.2811 Å in bulk ruthenium. The c/a ratio (1.64) is now close to the theoretical ratio of the hcp structure. The particles in CAC are agglomerated but contain particles of individual size displaying a broader size dispersion

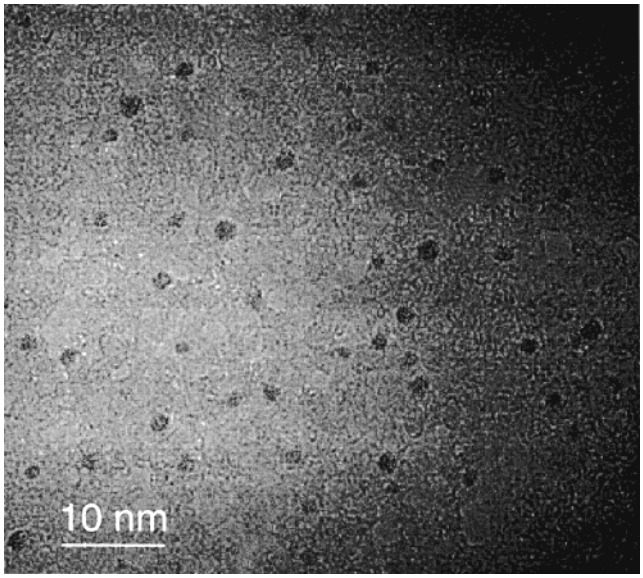

Figure 1. Transmission electron micrographs of ruthenium nanoparticles in PVP.

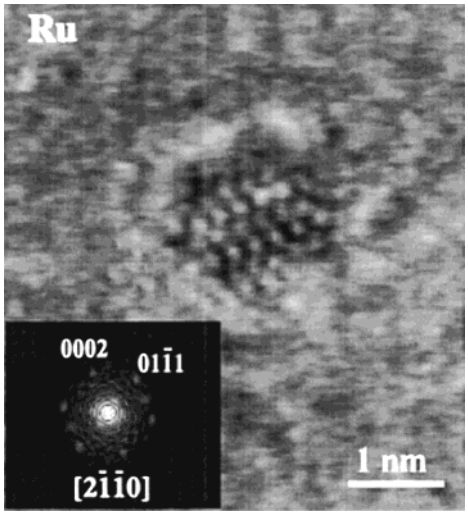

Figure 2. High-resolution electron micrographs of ruthenium nanoparticles in PVP.

(10) (a) Vidoni, O.; Philippot, K.; Amiens, C.; Chaudret, B.; Balmes, O.; Malm, J.-O.; Bovin, J.-O.; Senocq, F.; Casanove, M.-J. *Angew. Chem., Int. Ed.* **1999**, *38*, 3736. (b) Pan, C.; Dassenoy, F.; Casanove, M.-J.; Philippot, K.; Amiens, C.; Lecante, P.; Mosset, A.; Chaudret, B. *J. Phys. Chem. B* **1999**, *103*, 10098.

(11) (a) Respaud, M.; Broto, J. M.; Rakoto, H.; Fert, A. R.; Thomas, L.; Barbara, B.; Verelst, M.; Snoeck, E.; Lecante, P.; Mosset, A.; Osuna, J.; Ould Ely, T.; Amiens, C.; Chaudret, B. *Phys. Rev. B* **1998**, *57*, 2925. (b) Ould Ely, T.; Pan, C.; Amiens, C.; Chaudret, B.; Dassenoy, F.; Lecante, P.; Casanove, M.-J.; Mosset, A.; Respaud, M.; Broto, J. M. *J. Phys. Chem. B* **2000**, *104*, 695.

(12) Sun, S.; Murray, C. B.; Weller, D.; Folks, L.; Moser, A. *Science* **2000**, *287*, 1989.

(13) (a) Bönnemann, H.; Brijoux, W.; Brinkmann, R.; Fretzen, R.; Jounsen, T.; Köppler, R.; Neiteler, P.; Richter, J. *J. Mol. Catal.* **1994**, *86*, 129. (b) Liu, M.; Yu, W.; Liu, H. *J. Mol. Catal. A* **1999**, *138*, 295. (c) Lewis, L.N.; Lewis, L. *Chem. Mater.* **1989**, *1*, 106.

(14) Pertuci, P.; Vituli, G. *Inorg. Synth.* **1983**, *22*, 178.

(15) Duteil, A.; Quéau, R.; Chaudret, B.; Mazel, R.; Roucau, C.; Bradley, J. S. *Chem. Mater.* **1993**, *5*, 341.

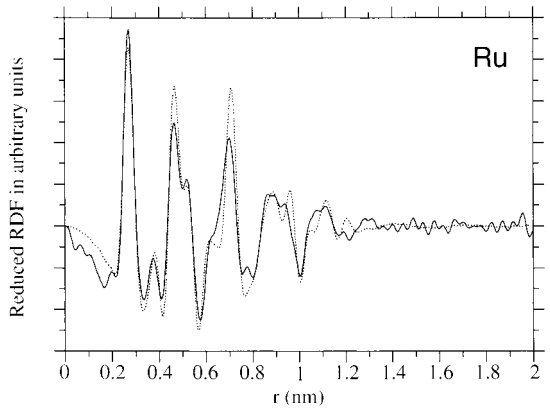

Figure 3. RDF of ruthenium nanoparticles in PVP.

and a larger mean size (1.7 nm). They also adopt the hcp structure of ruthenium, and the coherence length found by WAXS is in agreement with the size of the particles.

This study demonstrates that the decomposition of the precursor Ru(COD)(COT), in a medium which will poorly interact electronically with the surface of the particles but which is able to provide a good steric protection of the surface, yields crystalline nanoparticles of spherical appearance, small size, and narrow size distribution. In addition, infrared studies suggest a reduced surface state.

Stabilization of Ruthenium Particles by Amines

The reactions are carried out in a way similar to that described in the presence of a polymer: a solution of complex **1** was added to various quantities of an alkylamine in THF at 193 K. The resulting solution was then pressurized with 3 bar dihydrogen at 193 K and allowed to react for 20 h while the temperature was slowly raised to room temperature. A brown solution formed from which a black powder could be obtained after depressurization, concentration of the solution, and addition of pentane. The absence of residual amounts of **1** was monitored by column chromatography. This brown material can be washed with pentane and is soluble in THF. This procedure was applied for reactions of **1** with 0.2, 0.5, and 1 mole equiv of alkylamine ($C_8H_{17}NH_2$, $C_{12}H_{25}NH_2$, $C_{16}H_{33}NH_2$), leading to the production of nine different colloids, named **2**−**10**.

WAXS analysis was performed on all the colloids prepared in the presence of an amine except for **4**, which was found to be too sticky. In each case, the particles are crystalline and adopt the hcp structure of bulk ruthenium. A small deviation in the cell dimensions of the hcp network was observed as for the particles prepared in the presence of a polymer previously described and similarly indicative of the relaxation of the hcp structure. The coherence length is found above 2 nm, revealing a size larger than those found in polymers. Examples of RDF of colloids stabilized by hexadecylamine (colloids **8**−**10**) are given in Figures 4 and 5. They evidence the hcp structure of the particles and the similarity of coherence lengths for particles prepared using different quantities of amine.

The aspect of the particles as visualized by TEM and HREM depends on the ligand used. With 0.2 equiv of octylamine compared to ruthenium, individual spherical particles of mean diameter 2.3 nm are observed which are agglomerated into large spherical superstructures in the 100 nm range. In the presence of 0.5 equiv of octylamine, the size of individual particles does not seem to change much, but the particles are agglomerated into much larger and diffuse superstructures, which renders difficult their observation. The observation of particles was not possible for colloids prepared in the presence of larger amounts of octylamine.

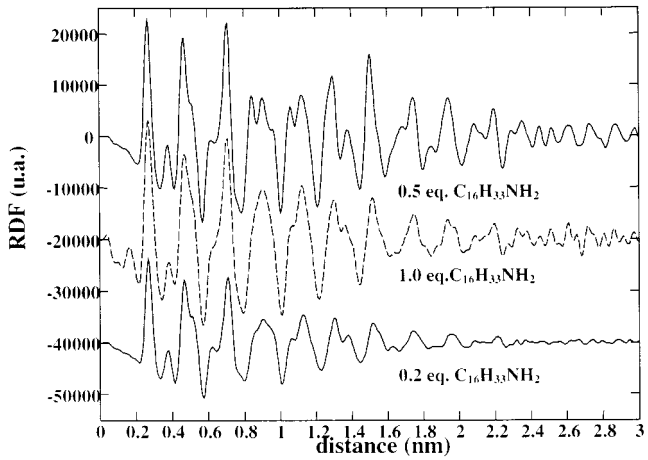

Figure 4. Experimental RDF of Ru particles stabilized by 0.2, 0.5, and 1 equiv of hexadecylamine (colloids **8**−**10**).

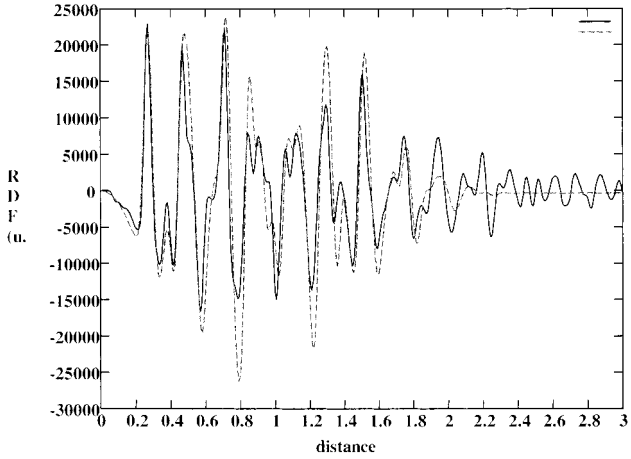

Figure 5. Comparison between a model of 396 atoms adopting the hcp ruthenium structure (- - -) and Ru particles (−) stabilized by 0.2 equiv of hexadecylamine (colloid **8**).

In the presence of a very low amount of hexadecylamine (0.04 equiv), a little soluble powder forms which displays agglomerated ill-defined nanoparticles of small size (ca. 1 nm) in TEM. However, in the case of both dodecyl- and hexadecylamine, with amine/ruthenium ratio equal to 0.2, 0.5, or 1, the particles display an unusual aspect. At the early stage of the reaction, when the amount of ligand is 0.2 equiv, the particles are well separated but have a tendency to be included in superstructures like recently reported for gold particles in hexadecylamine (Figures 6 and 7). The particles are monocrystalline, as evidenced by HREM analysis, and a careful observation of some electron micrographs reveals the presence of spherical particles which are in the process of coalescing (Figure 7). After some time in solution, the particles display an elongated or "vermicular" aspect (Figure 8). At high concentration of ruthenium in solution, for 0.5 equiv of amine the particles of colloid **9** seem to organize, as some areas displaying parallel rods were revealed (Figure 9). Upon increasing the relative concentration of the ligand compared to ruthenium, the aspect ratio of the particles decreased, and the particles were more agglomerated but still evidenced a tendency to form "worms". It is difficult to measure a size for such particles; however, we can measure a mean diameter of the "worms" (see Table 1). It is found to be regular for both the dodecyl- and the hexadecylamine ligands (near 1.8,

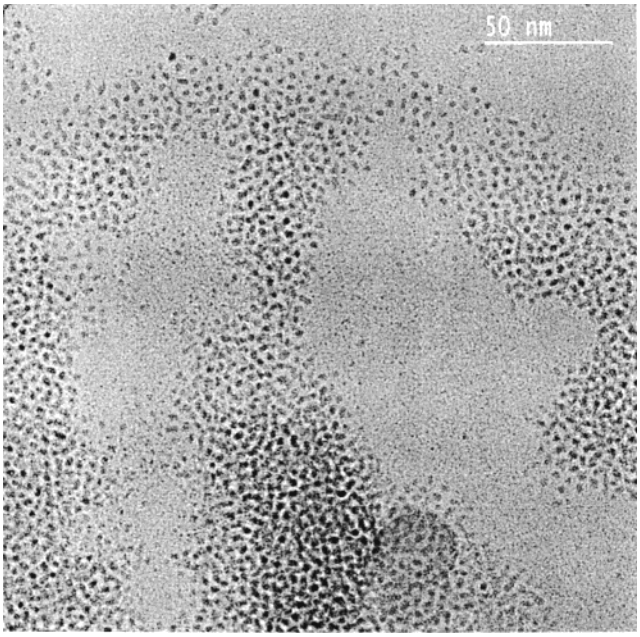

Figure 6. Transmission electron micrograph of colloid **8** (0.2 equiv of $C_{16}H_{33}NH_2$) at low concentration in THF.

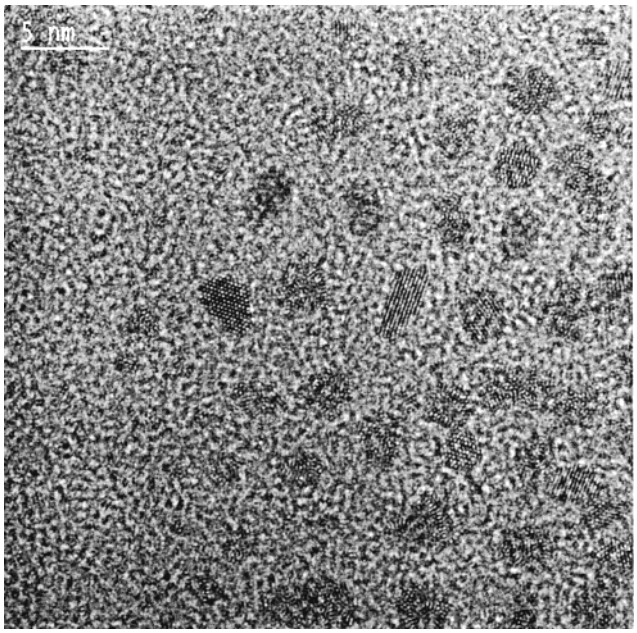

Figure 7. High-resolution electron micrograph of colloid **8** (0.2 equiv of $C_{16}H_{33}NH_2$) at low concentration in THF.

1.9 nm for 0.2 equiv of ligand, 2.3 nm for 0.5 equiv of ligand, and 2.3−2.6 nm for 1 equiv of ligand).

This vermicular aspect of the particles is surprising, as is their tendency to increase in diameter with increasing ligand concentration. This last result is in contrast with previous reports and with results obtained using thiol ligands and discussed further in this paper.[16] We therefore looked for a method which could shed some light on the coordination of the ligand at the surface of the particles since this could be a factor related to the shape of the particles. For this purpose we considered solution NMR, which has been previously used to demonstrate the mode of coordination and study the conformation of thiolate ligands at the surface of particles of gold.[9] We have also reported

(16) (a) Tian, F.; Klabunde, J. *New J. Chem.* **1998**, *22*, 1275. (b) Yonezawa, T.; Yasui, K.; Kimizuka, N. *Langmuir* **2001**, *17*, 271.

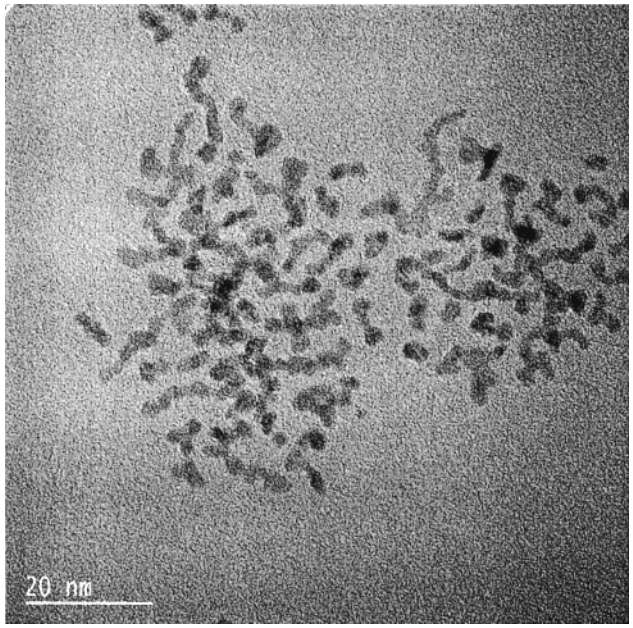

Figure 8. Transmission electron micrograph of colloid **8** (0.2 equiv of $C_{16}H_{33}NH_2$) showing the elongated aspect of the particles.

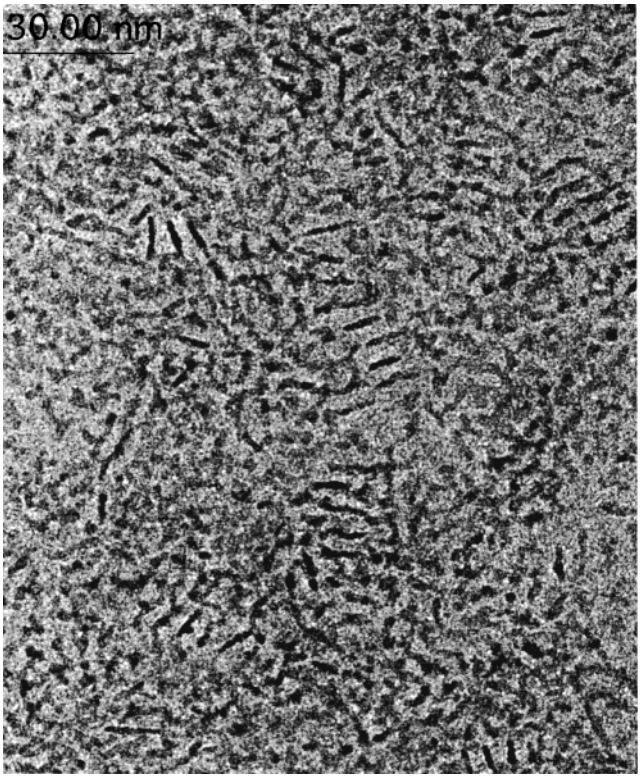

Figure 9. Transmission electron micrograph of colloid **9** (0.5 equiv of $C_{16}H_{33}NH_2$) at high concentration in THF.

the ^1H and ^{13}C NMR spectra of octanethiol-protected platinum nanoparticles which demonstrated the absence of dynamics between free and coordinated ligands.[4f] The study was carried out at room temperature in THF-d_8 (400 MHz for ^1H) on a representative purified sample, namely colloid **8** (0.2 equiv of $C_{16}H_{33}NH_2$). The ^1H NMR spectra show only the methyl groups of the ligands near 0.92 ppm and broad peaks for the methylene between 1.3 and 1.6 ppm but not the peaks attributed to the protons next to nitrogen. The ^{13}C NMR spectra are much more informative. Figure 10 shows the room-temperature spectrum of an isolated sample of colloid **8**, purified by precipitation and

Table 1. Summary of Results Obtained after Colloid Synthesis through Hydrogenation of Ru(COD)(COT) by 3 bar H_2 at Room Temperature

			size			
colloid	ligand (polymer)	molar ratio	TEM	WAXS[a]	shape	superstructure
	PVP		1.1	1.1	spherical	
	CAC		1.7	1.7	spherical	
2	$C_8H_{17}NH_2$	0.2	2.3	2.5	spherical	spherical agglomerates
3	$C_8H_{17}NH_2$	0.5		2.5	spherical	clouds
4	$C_8H_{17}NH_2$	1				
5	$C_{12}H_{25}NH_2$	0.2	1.8[b]	2.5	worms	
6	$C_{12}H_{25}NH_2$	0.5	2.3[b]	2.5	worms	
7	$C_{12}H_{25}NH_2$	1	2.3[b]	2.2	elongated	agglomerates
8	$C_{16}H_{33}NH_2$	0.2	1.9[b]	2.0	worms	
9	$C_{16}H_{33}NH_2$	0.5	2.4[b]	2.5	worms	organization of rods
10	$C_{16}H_{33}NH_2$	1	2.6[b]	2.5	elongated	
11	$C_8H_{17}SH$	0.2	2.3	2.3	spherical	spherical agglomerates
12	$C_8H_{17}SH$	0.5	ca. 2.5		spherical	
13	$C_8H_{17}SH$	1				
14	$C_{12}H_{25}SH$	0.2	*c*	2.3		spherical agglomerates
15	$C_{12}H_{25}SH$	0.5	*c*, ca. 2	1.8	spherical	spherical agglomerates
16	$C_{12}H_{25}SH$	1	*c*	1		spherical agglomerates
17	$C_{16}H_{33}SH$	0.2	*c*, ca. 2		spherical	cloudy
18	$C_{16}H_{33}SH$	0.5	*c*, ca. 2		spherical	
19	$C_{16}H_{33}SH$	1	*c*, ca. 1		spherical	

[a] Coherence length. [b] Diameter of the rods or "worms". [c] Difficult to measure due to the agglomeration.

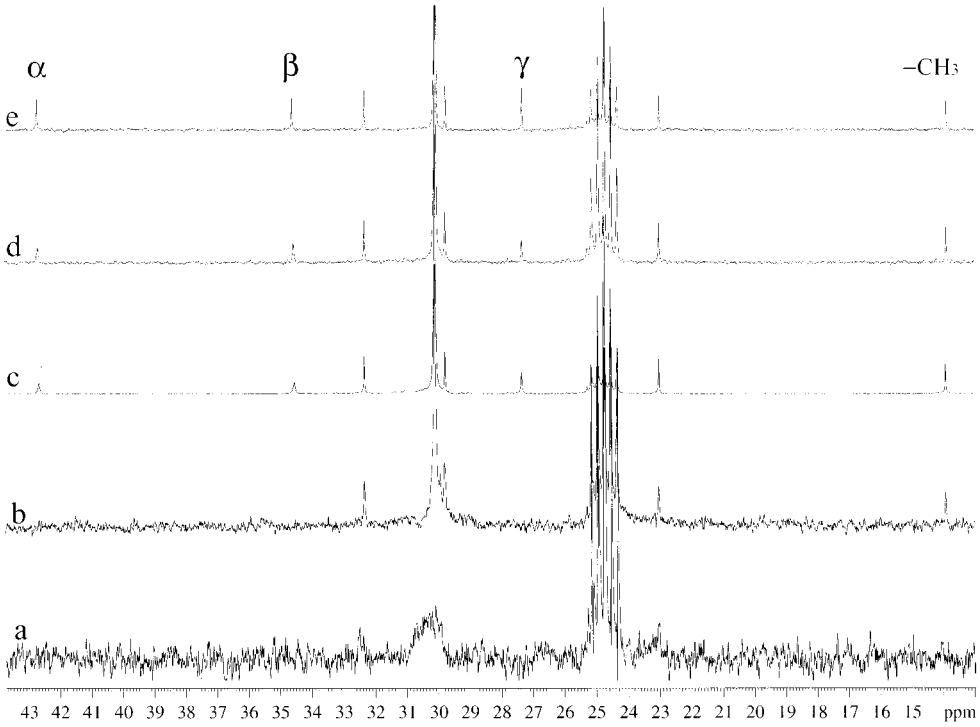

Figure 10. ^{13}C NMR spectra (THF-d_8, 101 MHz) of colloid **8** (a), colloid **8** + excess $C_{16}H_{33}NH_2$ (b−d), and $C_{16}H_{33}NH_2$ (e).

washing with pentane, as well as the effect of addition of known amounts of excess HDA and finally the spectrum of pure HDA, all recorded at 100.71 MHz, at the same temperature (303 K) and in the same solvent (THF-d_8). The first spectrum (a), corresponding to the initial isolated colloid, shows only three broad bands centered near 32.3, 30, and 23 ppm. These bands correspond to methylene groups of the alkyl chain of the amine, although both the carbons located in α, β, and γ positions relative to the amino group and, more surprisingly, the methyl group are not observed. An identical spectrum can be observed by preparing a colloid using 0.04 equiv of HDA relative to ruthenium. In this case, as stated above, small agglomerated nanoparticles are observed. Upon progressive addition of excess amine, we can observe (Figures 10 and 11) first in spectrum b the sharpening of the methylene peaks at 32.3, 29.8, and 23.0 ppm present in spectrum a, and the presence of a peak for the methyl group at 13.9 ppm, but no resonance for the α, β, and γ carbons. These peaks are relatively sharp but significantly broader than those in the free ligand and resonate at the same place as those of the free ligand. When additional amounts of hexadecylamine are added to colloid **8**, the peaks corresponding to the α, β, and γ carbons are now visible at 42.7, 34.5, and 27.3 ppm but with a half-height width broader than that of the other peaks and than that found for the peaks of the free ligand. Table 2 summarizes the data observed in different experiments. The interpretation of these results is the following: when only a small amount of HDA is present in solution, the α, β, and γ carbon resonances are missing because of the vicinity of the metal particle. This phenomenon has been previously observed on gold and platinum colloids and is attributed to chemical shift

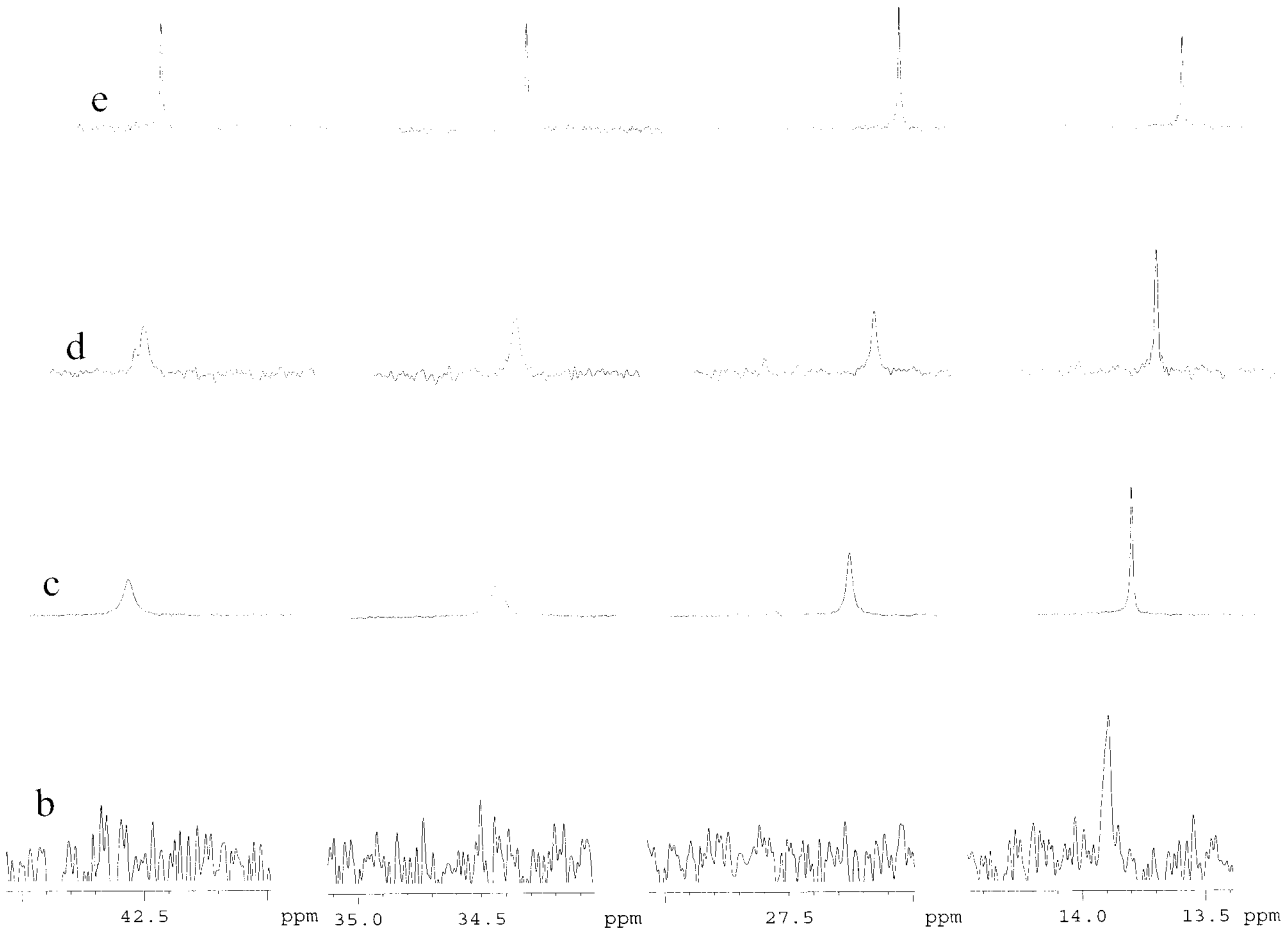

Figure 11. Enlargement of the spectra shown in Figure 10 b−e for comparison of line widths.

Table 2. ^{13}C NMR Data for Colloid **8** Evidencing the Modification of Half-Height Width in the Presence of Excess Free Ligand

carbon		α	β	γ	Me
chemical shift (ppm)		42.70	34.59	27.33	13.88
half-height width (Hz)	colloid **8**				4.2
	colloid **8** + 0.2 equiv of $C_{16}H_{33}NH_2$	4.8	6.4	2.5	0.9
	colloid **8** + excess $C_{16}H_{33}NH_2$	3.5	3.15	2.2	0.8
	free $C_{16}H_{33}NH_2$	0.9	0.92	0.69	0.65

anisotropy resulting from the slow tumbling of the particles in solution.[4f,9] Addition of excess ligand leads to the observation of these resonances (α, β, and γ carbons) but with a half-height width broader than that of the other peaks. Further addition of amine leads to the sharpening of these resonances. This observation is characteristic of a fast equilibrium on the NMR time scale between two species, in the present case free and coordinated amines. Attempts at lowering the temperature in order to observe a decoalescence of the exchange process failed because of precipitation of the colloids and of the ligands in the NMR tube. However, there is one more interesting observation: when a very small amount of ligand is present (Figure 10a), neither the α, β, and γ carbons nor the methyl group is observable, but some methylene carbons of the chain are observable. This suggests that for a very low HDA content, there may be a coverage of the ruthenium surface by the ligand and an interaction of the methyl group, perhaps through an agostic interaction, well-known in molecular chemistry. Addition of a small amount of HDA could then result in the displacement of this weak interaction by an amino group (Scheme 1) and therefore observation of the methyl group of HDA as a sharp singlet thanks to its fast tumbling at the end of the alkyl chain.

As a whole, this experiment evidences a rare example of observation of a dynamic process at the surface of metal nanoparticles by solution NMR. Precedents have been reported by Bradley on the dynamic exchange of ^{13}CO at the surface of palladium particles[17] and by Schmid on phosphine exchange at the surface of gold and rhodium particles.[18] The originality of the present system lies in the observation of both the spectra for coordinated ligands and those for the rapid exchange.

Stabilization of Ruthenium Particles by Thiols

A procedure similar to that described above with amines can be applied for reacting **1** with 0.2, 0.5, and 1 mole equiv of an alkanethiol ($C_8H_{17}SH$, $C_{12}H_{25}SH$, $C_{16}H_{33}SH$), leading to the production of nine different colloids named **11**−**19**. In the case where 1 mole equiv of thiol compared to **1** was used, the precipitates obtained were sticky, and the corresponding colloids **13**, **16**, and **19** could not be purified.

WAXS analysis was performed on colloids prepared in the presence of 0.2 equiv of octanethiol (**11**) and on all samples prepared in the presence of dodecanethiol (**14**−**16**). In each case, as for **2**−**10**, the particles were found to be crystalline and to

(17) Bradley, J. S.; Millar, J.; Hill, E. W. *J. Am. Chem. Soc.* **1991**, *113*, 4016.

(18) (a) Schmid, G.; Giebel, U.; Huster, W.; Schwenk, A. *Inorg. Chim. Acta* **1984**, *85*, 97. (b) Schmid, G. *Struct. Bonding* **1985**, *62*, 51.

Scheme 1. Possible Ways of Coordination of Hexadecylamine on Ruthenium Particles as a Function of Amine Concentration

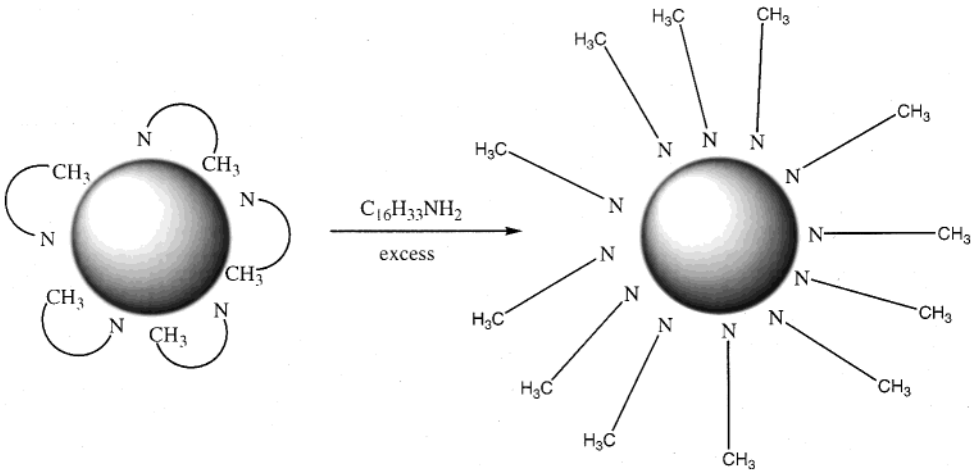

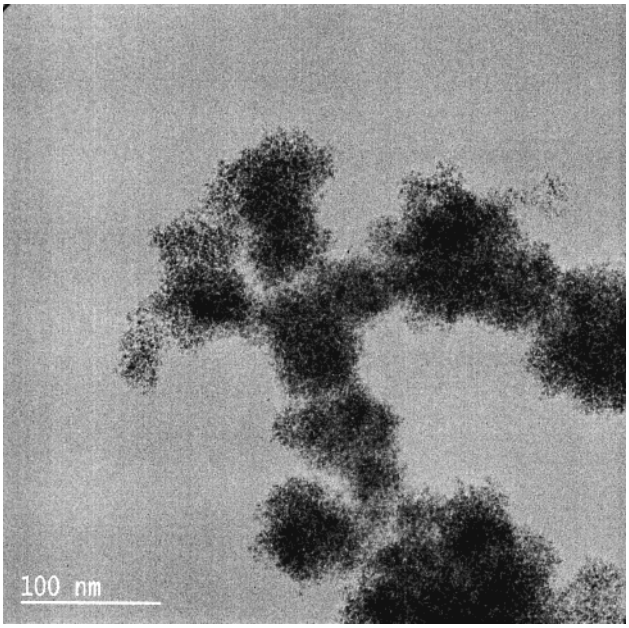

Figure 12. Transmission electron micrograph of colloid **11** (0.2 equiv of $C_8H_{17}SH$).

adopt the hcp structure of bulk ruthenium with the same small deviation in the cell dimensions of the hcp network previously discussed. The RDF of colloids **14**−**16** evidences the same hcp structure as for the particles prepared in the presence of amines but, in contrast to the observation for colloids **8**−**10**, a net decrease in the coherence length as the concentration of dodecanethiol is increased.

TEM and HREM analysis evidenced the presence of crystalline particles adopting the hcp structure and of spherical aspect. The size of these particles decreased as the ligand concentration increased, as indicated by WAXS experiments and previously observed.[16] The size of the particles remained, however, near 2−3 nm except for colloid **14** (0.2 equiv of dodecanethiol), for which it was found to be between 5 and 10 nm. The particles prepared in the presence of octane- and dodecanethiol were found to be strongly agglomerated and included into superstructures in some cases (0.2 equiv of octanethiol, colloid **11** for example, see Figure 12). In the presence of 0.5 or 1 equiv of hexadecanethiol, however, probably because of the chain length, no agglomeration was observed, but individual particles of spherical aspect were observed. The size of the particles varies from 2.3 nm for colloid **11** to ca. 1 nm for colloid **19**.

The observation of agglomerated particles is in marked contrast with the observation that nanoparticles of comparable size of gold or of platinum are perfectly stabilized by the same ligands (octanethiol, dodecanethiol), do not agglomerate, and can be deposited as monolayers on various substrates.

Since this behavior was again found intriguing, a solution NMR study was undertaken. The study was carried out at room temperature in THF-d_8 (400 MHz for ^{1}H) on colloid **11** (0.2 equiv of $C_8H_{17}SH$). As for colloid **8**, attempts at lowering the temperature resulted in the precipitation of the colloid and of the excess ligand. The ^{1}H NMR spectra show only, as previously described for colloid **8**, peaks for the methyl groups of the ligands near 0.92 ppm and broad peaks for the methylene between 1.3 and 1.6 ppm, but not the peaks attributed to the protons next to sulfur. The ^{13}C NMR spectra show the peaks corresponding to the carbons of the ligands coordinated to the nanoparticle (Figure 13, spectrum b). They are broad and, as expected, at least two peaks corresponding to the α and β carbons are missing for the same reasons as previously described for colloid **8**. However, when an excess of free thiol (ca. 7 equiv compared to the amount of coordinated ligand) is added to the solution, we see the appearance, next to the colloid peaks, of sharp signals which are very close to those of the free ligand for all carbons but one, the α carbon, which resonates at 34.7 ppm for $C_8H_{17}SH$ but is found here at 39.0 ppm. This shift results from the transformation of the thiol into the disulfide $C_8H_{17}S_2C_8H_{17}$. This reaction could be monitored by ^{1}H NMR, where we could follow the transformation of the quartet at 2.50 ppm resulting from the protons located on the α carbon in $C_8H_{17}SH$ into a triplet at 2.70 ppm for the corresponding protons in $C_8H_{17}S_2C_8H_{17}$. These experiments therefore demonstrate the catalytic oxidation of a thiol into a disulfide at the surface of ruthenium nanoparticles. This could result in the formation of disulfide-protected particles as recently reported for gold,[19] or even in metal precipitation after decoordination of all disulfide ligands. However, the colloids are stable, and if the ligands which are present at the surface of the colloids are disulfides, they do not rapidly exchange at the NMR time scale with the free ligands.

Two mechanisms can account for this transformation: the catalytic coupling of thiolate ligands, leading to the production of dihydrogen, or the air oxidation catalyzed by platinum and producing water as a byproduct. An important observation is the detection of free dihydrogen by ^{1}H NMR at the early stage

(19) Porter, L. A., Jr.; Ji, D.; Westcott, S. L.; Graupe, M.; Czernuszewicz, R. S.; Halas, N. J.; Lee, T. R. *Langmuir* **1998**, *14*, 7378.

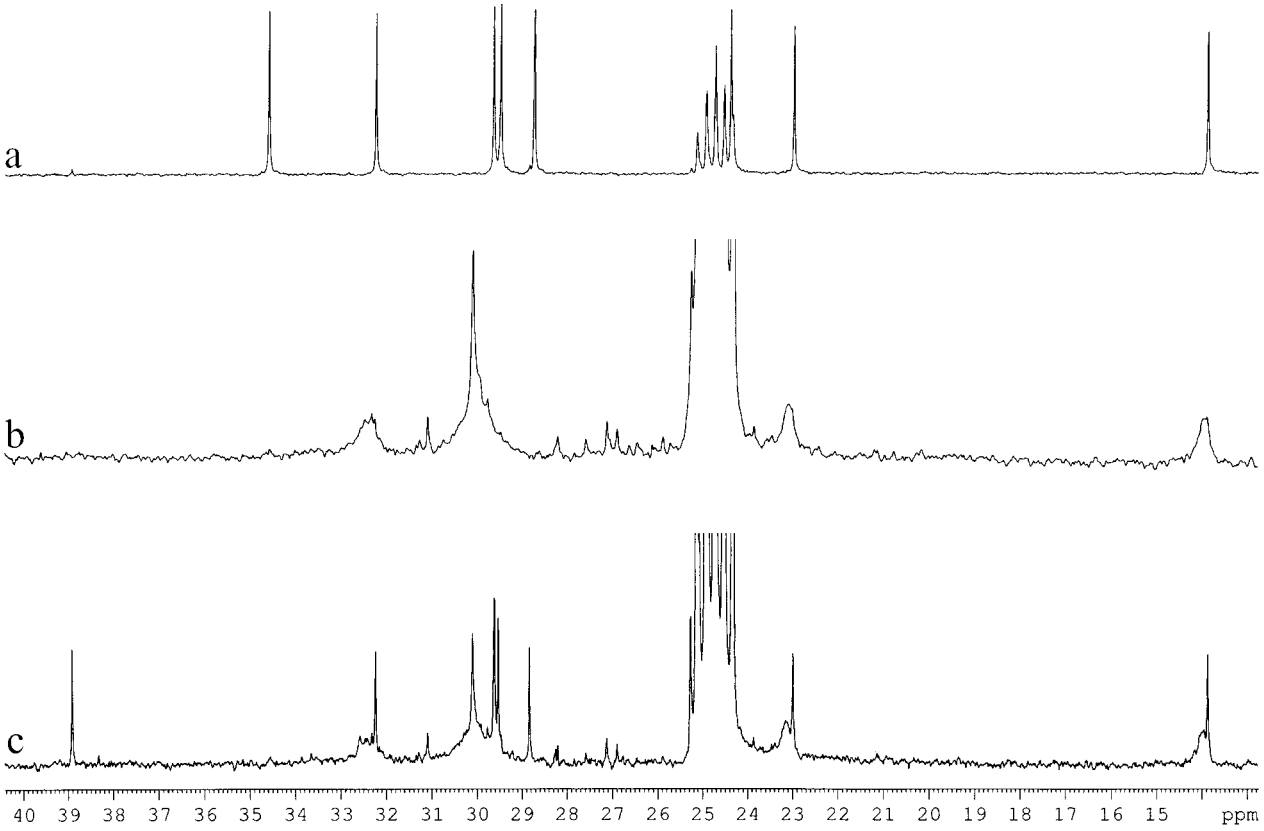

Figure 13. ^{13}C NMR spectra (THF-d_8, 101 MHz) of $C_8H_{17}SH$ (a), colloid **8** (b), and colloid **8** + excess $C_8H_{17}SH$ (c).

of the reaction.[20] Dissolved H_2 was identified by its chemical shift (4.8 ppm in THF-d_8) and its long relaxation time (T_1 = 2.1 s). The spectrum is broad but sharpens when the temperature of the sample is cooled to 293 K. As stated above, further cooling resulted in the precipitation of the colloid. This line width results from an equilibrium, detectable on the NMR time scale, between dissolved H_2 and H_2O present in the solution which demonstrates the ability of the particles to split H−H and H−O bonds. This process could not be studied thoroughly because of the elimination of H_2 from the reaction solution: as the H_2 concentration decreases, the shape of the spectrum changes and the H_2 peak vanishes. It has therefore not been possible to observe the formation of H_2 during the catalytic coupling of thiols, probably because the reaction is very slow and the concentration of H_2 in solution remains very low. To test the alternative oxidation mechanism, two parallel reactions between the ruthenium colloid and excess hexadecanethiol were carried out, one in a rigorously controlled atmosphere, and the other like the first one but with air (ca. 500 μL) injected in the solution just before the first NMR spectrum was run. In the first case, we observed the catalytic coupling reactions; in the second one, in the presence of air, the reaction was frozen. This demonstrates that the coupling needs a controlled atmosphere and involves oxidative addition of thiol followed by reductive elimination of disulfide and dihydrogen. In this respect, the initial observation of dissolved H_2 most probably results from the oxidative addition of thiols on a ruthenium particle, producing surface hydrides, and from the recombination of two of these hydrides. The elimination of H_2 from the reaction solution may be a driving force for the coupling.

This NMR study demonstrates the oxidative addition of thiols to the ruthenium particles' surface and the elimination of surface hydride (or dihydrogen) ligands resulting from the colloid synthesis. When excess thiol is present, a catalytic coupling of thiol into disulfide, slow on the NMR time scale, is observed.

Conclusion

In summary, ruthenium nanoparticles are easily prepared at room temperature by hydrogenation of the organometallic precursor Ru(COD)(COT). Polymers can be used as stabilizers, in which case well-dispersed nanoparticles of small size (near 1 nm) and of classical spherical shape are obtained. The particles can also be stabilized by long-chain amines or thiols to give after appropriate workup colloids which can be obtained as powders and handled like organometallic compounds. Whereas the amine ligands exchange rapidly at the surface of the particles with free amines, the thiols oxidatively add to ruthenium, and excess thiol leads to the reductive elimination of disulfides which are released into the solution and do not exchange with the ligands present at the surface of the particles. This may be the reason why the colloids adopt such different structures and superstructures, even though the alkyl chains are the same and the functional groups are similar. Thus, the alkyl chains of the sulfur ligands will encircle the particle and interpenetrate with the alkyl chains of other ligands that are either free or located at the surface of other particles, hence leading to the formation of superstructures. The observation of a slow catalytic coupling of thiols into disulfides which may be removed from the colloid surface is in agreement with recent observations demonstrating that the removal of ligands from the surface of gold particles force the particles to organize into superstructures.[21] It is difficult to determine whether this phenomenon is occurring in our case.

(20) *J. Catal.* **1990**, *121*, 271.

(21) Schmid, G.; Meyer-Zaika, W.; Pugin, R.; Sawitowski, T.; Majoral, J.-P.; Caminade, A.-M.; Turrin C.-O. *Chem. Eur. J.* **2000**, *6*, 1693.

It is, however, noteworthy that platinum particles of similar sizes do not aggregate when octanethiol is employed.[4f] In contrast, the dynamics of the amine at the surface of the particle may allow the self-organization of these amines, which are known to produce in water micellar arrangements and even hexagonal phases used for templating the synthesis of mesoporous materials.[22] The presence of some organization of the amines in THF could allow the growth of ruthenium particles in the channel created in this way and hence explain the vermicular aspects of colloids **5**−**10**. Alternatively, the dynamics of the amines could also allow changes in the coordination sites at the surface of the particles and, therefore, the preferred coordination of the amine along the growth axis of the hcp structure, perpendicular to the basal plane. In any case, the dynamics of the amine will favor the coalescence of initially formed spherical particles and therefore favor the formation of wormlike particles. This appears particularly clearly in Figure 7.

This study demonstrates that the coupling of traditional techniques of characterization of nanomaterials (HREM, WAXS) with simple techniques of organometallic chemistry may provide useful information on the chemical reactivity of the surface of the nanoparticles and shed light on elementary surface reaction steps such as substitution, oxidative addition, and reductive elimination. Such a study may also help in designing nanoparticles of defined shape and organization at the mesoscopic level. Finally, it is, to our knowledge, one of the very few NMR studies evidencing such processes as dynamic ligand exchange and catalytic coupling of thiols at the surface of metal nanoparticles, and probably the first one relating the dynamics of coordinated ligands to the shape of the particles.

Experimental Section

Typical Synthetic Procedures. All colloid syntheses were carried out in the same way. We describe here typical experiments using a polymer, an amine, or a thiol as stabilizers.

(i) Synthesis of Ruthenium Colloids Stabilized by PVP. Ru(COD)(COT) (158 mg, 0.50 mmol) was introduced in a Fischer−Porter bottle and left in vacuo for 30 min. A solution of 1 g of PVP in 60 mL of THF, degassed by freeze−pump cycles, was then added using a transfer tubing. The resulting yellow solution was stirred for 30 min at room temperature, after which the bottle was pressurized under 3 bar dihydrogen and the solution allowed to react for 68 h, during which time a black precipitate formed. After elimination of excess dihydrogen, the solution was filtrated and the black precipitate dried in vacuo. The precipitate was then redissolved in 30 mL of methanol, and the resulting solution was filtrated and reduced to 15 mL, after which addition of 30 mL of pentane led to a dark brown precipitate. It was filtered, washed with pentane, and dried in vacuo.

Ru content of the powder: 7.61 wt %.

A similar procedure was used for the reaction in the presence of CAC, using 1 g of CAC.

Ru content of the powder: 4.34 wt %.

(ii) Synthesis of Colloid 8. Ru(COD)(COT) (158 mg, 0.50 mmol) was introduced in a Fischer−Porter bottle and left in vacuo for 30 min. Next, 125 mL of THF, degassed by freeze−pump cycles, was added. The resulting yellow solution was cooled at 193 K, after which a solution of 26 mg (0.10 mmol) of hexadecylamine in 25 mL of THF was introduced in the flask. The bottle was pressurized under 3 bar dihydrogen and the solution allowed to warm slowly to room temperature. After 20 h, a homogeneous brown solution was obtained. After elimination of excess dihydrogen, ca. 3 mL of the solution was passed under argon over a small alumina column. The absence of color of the filtrate indicates the full decomposition of the precursor. The volume of the solution was then reduced to ca. 15 mL, 50 mL of pentane was added, and the resulting mixture was cooled to 193 K, at which temperature a brown precipitate formed. It was filtered, washed with pentane, and dried in vacuo.

All other syntheses were performed using the same procedure with 158 mg of **1**, 3 bar H_2, a reaction time of 20 h, and an initial temperature of −80 °C. The other conditions and microanalysis results are as follows:

colloid	ligand concentration (theoretical)	amount of added ligand	volume of THF (mL)	microanalysis (%) Ru	N
2	0.2 equiv $C_8H_{17}NH_2$	17 μL	30	62.24	1.07
3	0.5 equiv $C_8H_{17}NH_2$	42 μL	30	83.03	1.85
5	0.2 equiv $C_{12}H_{25}NH_2$	18.6 mg	150	69.22	1.64
6	0.5 equiv $C_{12}H_{25}NH_2$	47.5 mg	30	79.8	
7	1 equiv $C_{12}H_{25}NH_2$	94.8 mg	30		
8	0.2 equiv $C_{16}H_{33}NH_2$	26 mg	150	53.2	1.45
9	0.5 equiv $C_{16}H_{33}NH_2$	61 mg	150	52.53	2.65
10	1 equiv $C_{16}H_{33}NH_2$	122 mg	30		

(iii) Synthesis of Colloid 11. Ru(COD)(COT) (158 mg, 0.50 mmol) was introduced in a Fischer−Porter bottle and left in vacuo for 30 min. Next, 125 mL of THF degassed by freeze−pump cycles was added. The resulting yellow solution was cooled at 193 K, after which a solution of 17 μL (0.10 mmol) of octanethiol in 25 mL of THF was introduced in the flask. The bottle was pressurized under 3 bar dihydrogen and the solution allowed to warm slowly to room temperature. After 20 h, a brown suspension was obtained. After elimination of excess dihydrogen, ca. 3 mL of the solution was passed under argon over a small alumina column. The absence of color of the filtrate indicates the full decomposition of the precursor. The volume of the solution was then reduced to ca. 15 mL, 50 mL of pentane was added, and the resulting mixture was cooled to 193 K, at which temperature a brown precipitate formed. It was filtered, washed with pentane, and dried in vacuo.

All other syntheses were performed using the same procedure with 158 mg of **1**, 3 bar H_2, a reaction time of 20 h, and an initial temperature of −80 °C. The other conditions and microanalysis are as follows:

colloid	ligand concentration (theoretical)	amount of added ligand	volume of THF (mL)	microanalysis (%) Ru	N
11	0.2 equiv $C_8H_{17}SH$	17.5 μL	150	80.52	5.62
12	0.5 equiv $C_8H_{17}SH$	43.5 μL	150	69.34	9.03
14	0.2 equiv $C_{12}H_{25}SH$	24 μL	150	79.72	5.48
15	0.5 equiv $C_{12}H_{25}SH$	60 μL	30	65.25	7.05
16	1 equiv $C_{12}H_{25}SH$	120 μL	30		
17	0.2 equiv $C_{16}H_{33}SH$	28 mg	30	67.94	4.83
18	0.5 equiv $C_{16}H_{33}SH$	70.5 mg	150	56.83	5.89
19	1 equiv $C_{16}H_{33}SH$	141 mg	30		

NMR Characterization. NMR spectra were recorded in THF-d_8 on a Bruker AMX 400 operating at 400 MHz in ^{1}H NMR and 100.71 MHz in ^{13}C NMR.

TEM and HRTEM Experiments. The TEM specimens were prepared by slow evaporation in a glovebox of droplets of diluted solutions of the different colloids deposited on a high-resolution carbon-supported copper grid. The experiments were performed on a Philips CM 30/ST operated at 300 kV with point resolution 0.19 nm.

The size distribution was measured through the numerical analysis of TEM low-magnification images. In this procedure, the different particles were first identified according to an upper and lower intensity threshold and then counted and measured. Histograms of the size distribution (not shown) include the measurement of about 300 particles and were reproduced in different regions of the samples. HRTEM images of isolated particles were digitized at a resolution of 0.03 nm/pixel and analyzed using their numerical diffractograms (Fourier transforms).

WAXS Experiments. Data collection was performed on small amounts of powder (obtained after drying) sealed in 1.5-mm-diameter

(22) (a) Tanev, P. T.; Pinnavaia, T. J. *Science* **1996**, *271*, 1267. (b) Ulagaappan, N.; Battaram, N.; Rraju, V. N.; Rao, C. N. R. *J. Chem. Soc., Chem. Commun.* **1996**, 2243.

Lindemann glass capillaries after filling in a glovebox. Measurements of the X-ray intensity scattered by the samples irradiated with graphite-monochromatized molybdenum Kα (0.071069 nm) radiation were performed using a dedicated two-axis diffractometer. Time for data collection was typically 20 h for a set of 457 measurements collected at room temperature in the range $0° < \theta < 65°$ for equidistant s values ($s = 4\pi(\sin\theta/\lambda)$†). The raw intensity was corrected for contributions generated by other components (polymer, empty capillary) attenuated by sample absorption. Air scattering background was small enough to be neglected. Polarization and self-absorption corrections were also applied. Data were reduced in order to extract the structure-related component of WAXS, the so-called reduced intensity function, normalized to a number of atoms corresponding to the size of the particle, and Fourier transformed to allow for radial distribution function (RDF) analysis, using

$$F(r) = \frac{2r}{\pi}\int_{S_{\min}}^{S_{\max}} si(s)\sin(rs)\,\mathrm{d}s$$

where $F(r)$ is actually a reduced RDF whose maximum for a given r value indicates that at least two atoms in an elementary volume are separated by the distance r. Analysis of the experimental results provided an approximate measurement of the metal−metal bond length and of the order extent inside the particles. To further investigate the structure, different models were defined in order to compute theoretical functions for intensity and radial distribution via the Debye formula:

$$i_D(s) = 2\sum_{i=1}^{N-1}\sum_{j=i+1}^{N} f_i(s)f_j(s)\frac{\sin(sr_{ij})}{sr_{ij}}\exp(-b_{ij}s^2)$$

where N is the total number of atoms in the model, f_i the atomic scattering factor for atom i, r_{ij} the distance between atoms i and j, and b_{ij} a dispersion factor affecting the $i-j$ interaction).

The best values of the parameters defining the models were estimated from the agreement reached between experimental and computed RDF, both normalized to one atom, but also between the related reduced intensity functions.

Acknowledgment. The authors thank CNRS for support and Dr. Y. Coppel for NMR spectra.

Supporting Information Available: Experimental and characterization data (PDF). This material is available free of charge via the Internet at http://pubs.acs.org.

JA003961M